Subcritical Detection of an Elongated Target Buried Under a Rippled Interface

C. L. Nesbitt and J. L. Lopes
Naval Surface Warfare Center – Panama City
Code R21
110 Vernon Ave.
Panama City, FL 32407-7001

***Abstract*- This paper describes recent results from an on-going measurement and modeling effort investigating shallow grazing angle acoustic detection of targets buried under a rippled bottom. The measurements are being performed in a 13.7-m deep, 110-m long, 80-m wide test-pool with a 1.5-m layer of sand on the bottom. The rippled bottom is formed by scraping the sand with a machined rake. A parametric sonar (1 to 20 kHz) and broad band (10 to 50 kHz) transducers are placed onto the shaft of a tilting motor, which in turn is attached to an elevated rail that enables this assembly to be translated horizontally, permitting acquired data to be processed and displayed as images. Data acquired with the broad band transducers could be further processed using synthetic aperture sonar (SAS) techniques. In previous work, measured calibrated backscatter levels obtained from a buried silicone oil-filled sphere were compared to predictions of a model that uses perturbation theory. Most of the data-model comparisons exhibited good agreement (Lopes et al., "Subcritical Detection of Targets Buried Under a Rippled Interface: Calibrated Levels and Effects of Large Roughness," MTS/IEEE, pp.485-493.). In order to evaluate model predictions on more complex scatterers, an additional series of measurements was conducted using an elongated cylindrical shaped target that was buried under the rippled surface. Images of the buried cylindrical target were generated and are presented. Also presented are signal-to-noise ratios of the buried target.**

I. INTRODUCTION

Coastal areas present unique challenges to Mine Countermeasure (MCM) operations. Due to the close proximity of the sea surface and sea bottom, wave-induced effects are significant near the sea bottom, and objects such as mines placed on the sea floor may bury. In order to obtain large standoff distances and high area-coverage rates with sonar, buried targets need to be detected at shallow grazing angles. For sand sediments, where the speed of sound is higher than in the water, this implies the need for detection below the critical grazing angle ("subcritical" grazing angle detection).

Physical models, treating sandy sediments as an attenuating fluid with a flat interface, predict little to no acoustic penetration into sand at subcritical grazing angles. However, recent research has demonstrated that a roughened bottom interface will enhance subcritical penetration. A bottom interface with a random roughness will permit limited penetration, but the dominant mechanism for subcritical penetration appears to be due to scattering from ripple on the water-sediment interface.[1] Ripple acts as a diffraction grating that produces a "quasi-coherent" propagating wave in the sediment.

N^{th}-order perturbation theory predicts that the maximum depression angle (β_n) of the n^{th}-order field propagating in the sediment due to scattering from periodic ripples is given by

$$\cos\beta_n = \frac{C_2}{C_1}\left(\cos\theta - \frac{n\lambda}{\lambda_r}\right). \qquad (1)$$

Here, C_1 is the water sound speed, C_2 is the sediment sound speed, θ is the incident grazing angle, λ is the acoustic wavelength in water, and λ_r is the ripple wavelength.

Recently, a controlled set of measurements was conducted to investigate subcritical detection of targets buried under a rippled interface.[2,3] In these measurements, a silicone-oil-filled sphere was buried under various sinusoidal shaped interfaces with wavelengths of 50 cm and 75 cm and root-mean-square (RMS) heights about the mean of 1.6 cm and 2.5 cm. In each case, the ripple wave vectors were oriented in the same direction as the projected acoustic beam. This initial set of measurements demonstrated subcritical detection via ripple scattering. In addition, models that use first-order perturbation theory to determine shallow grazing angle penetration were shown to capture much of the behavior of the data. Measured calibrated backscattered levels were found to be in good agreement with model predictions across the experimental bandwidth of 10 to 50 kHz. However, exceptions to this agreement with low-order perturbation theory appear when the ripple amplitude is high.

The objective of this effort is to conduct a controlled set of laboratory-type measurements investigating the acoustic detection of targets buried under a rippled interface at subcritical grazing angles under more realistic conditions. In this effort, a series of controlled measurements are conducted to determine the effects of ripple orientation on detection performance of a cylindrical /extended target in the frequency range of 1 kHz to 50 kHz. Results of these measurements are presented in this paper.

II. MEASUREMENT SETUP

The measurements reported here were conducted in the Naval Surface Warfare Center – Panama City (NSWC-PC) Facility 383 over the course of several months (February through May 2004). NSWC-PC Facility 383 is a fresh-water test pool that is 13.7 m deep, 110 m long, and 80 m wide with approximately 1.5 m of sand covering the bottom. A filtration system provided approximately 12 m (~ 40 ft) water visibility and mixed the water column. The sound speed in the water was found to have no velocity gradients, and it varied from 1461 m/s in February to 1507

m/s in May. The bottom sediment was characterized to have an attenuation level of about 0.33 dB/kHz/m, which is typical of sands, and a sound speed of 1668 m/s when the corresponding water sound speed was 1482 m/s. Using the measured in-water and in-sediment sound velocity, and a porous sediment model[4] for sound propagation in the sediment, the critical grazing angle was calculated to range from 26^o to 26.5^o.

Figure 1 depicts the target field viewed from directly overhead. The target field contained a rippled bottom area, a buried target, a rail system with a sonar tower and an extender, projectors, backscatter receivers, and free-field hydrophones. In addition, a sand-scraping apparatus was used to create sinusoidal ripple profiles on the bottom sediment over the buried target. The rippled profile of the scraped bottom patch and the superimposed fine-scale roughness were measured using the In-situ Measurement of Porosity 2 (IMP2) system. (An early version of IMP2 is described in [5].) Each of these components is described below.

The buried target was a solid aluminum cylinder with a 30.5-cm (12-inch) diameter and 1.52 m (5 ft) length. The target was buried by divers with the aid of a dredge pump-system. The target was buried approximately 10 cm below the water-sediment interface at a range of almost 10.3 m from the rail system. The cylinder was buried under the rippled bottom at a target aspect angle near broad side.

For each ripple profile, the burial depth of the target relative to the mean sand surface and its aspect angle with respect to the rail system were measured (after collection of all acoustic data) by divers with the aid of a reference bar and probe. The cylinder was found to be approximately 6.5^o off broad side and the top of the cylinder was buried by about 10.8 cm below the mean ripple height for each of the three ripples formed. Depth uncertainties are estimated to be ± 1cm and horizontal uncertainties to be ± 5 cm.

The rippled bottom area was a patch approximately 3.66 m (12 ft) in length by 3.66 m (12 ft) in width, and it started about 8.3 m from the rail system (see Fig. 1). The scraper used to form the ripple consisted of a frame and a "rake" that glided along the frame. Divers positioned the sand scraper at the appropriate range and angular orientation from the rail system with the aid of specified lengths of wire rope that ran between the rail system and the sand scraper. After positioning the sand scraper, divers removed the wire ropes and attached concrete blocks (each weighed almost 2000 lbs) to each corner of the sand scraper to hold it in place. The rake was then pulled across the sand using two winches located on each side of the test pool. Attaching different inserts to the rake could form different ripple contours. In the work reported in this paper, three sinusoidal profiles corresponding to ripple orientations of 0^o, 17^o, and 31^o were formed. Each profile was designed to have a ripple wavelength of 75 cm with an RMS height of 2.7 cm (as verified by measurements utilizing the IMP2). After forming each ripple, divers carefully removed the sand scraper and concrete blocks from the target field so as not to disturb the formed bottom.

The bottom contour and fine-scale roughness parameter over the buried target were measured with the IMP2. Figure 2 shows the three different measurements of the ripple profiles by IMP2. Above the wavenumber associated with each ripple wavelength, a power law was fit to the roughness spectrum to characterize fine-scale roughness, resulting in an estimated two-dimensional power-law spectrum for each ripple configuration. Table 1 lists the IMP2 measured ripple RMS height for each ripple configuration and the computed spectral exponent, γ_2, and spectral strength,[6] w_2, for the fine-scale features superimposed on each ripple configuration.

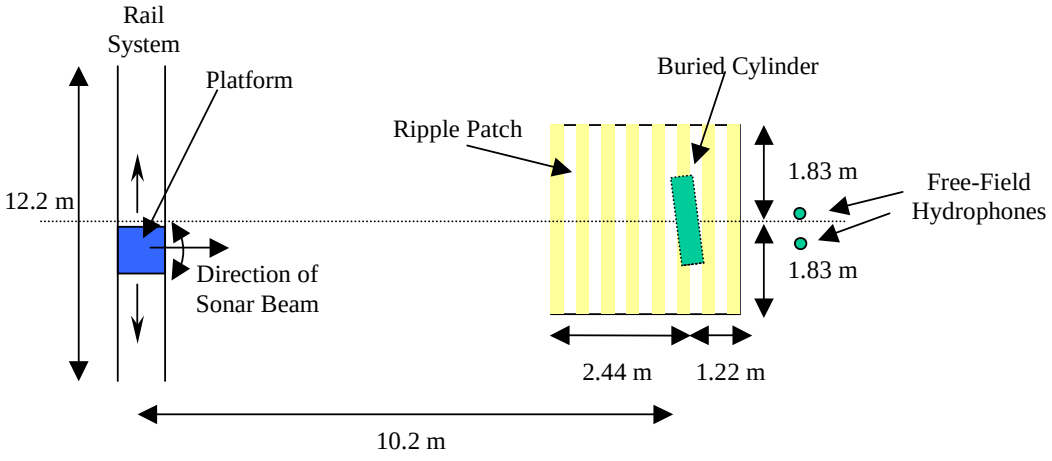

Fig. 1. Target field.

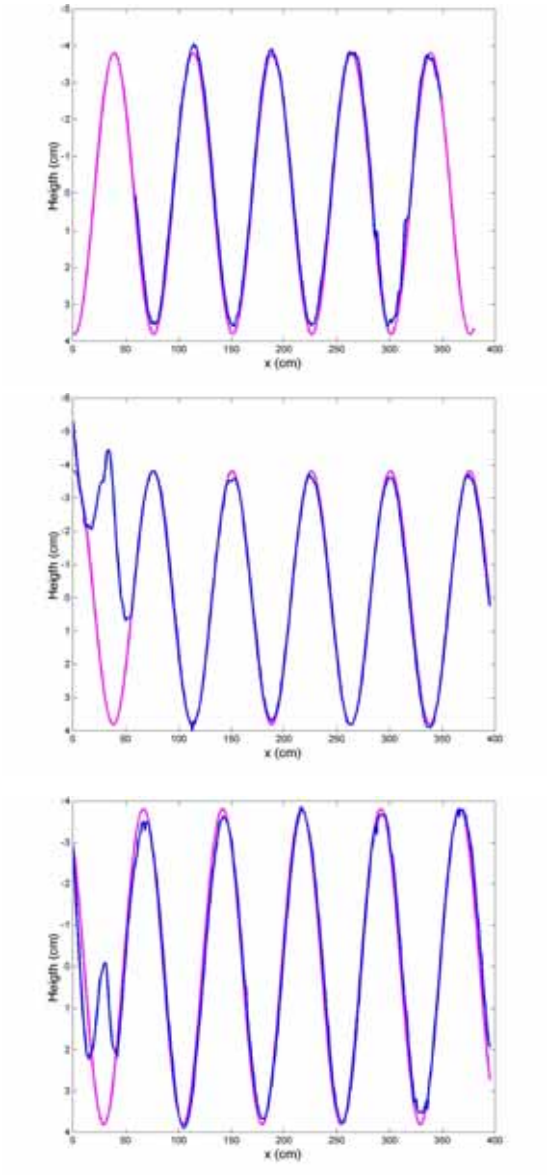

Fig. 2. Designed (red) and IMP2 measured (blue) ripple profiles for 0^o (top), 17^o (middle), and 31^o (bottom) ripple orientations.

Table 1. IMP2 measured ripple parameters.

Orientation	RMS Height	γ_2	w_2 (cm$^{(4-\gamma_2)}$)
0^o	2.66 cm	2.57	0.0001861
17^o	2.58 cm	2.16	0.0001304
31^o	2.64 cm	3.07	0.0001336

A rail system was also employed in the measurement and permitted data acquisition from different parts of the target field so data could be displayed as an image and synthetic aperture sonar (SAS) processing could be applied. A photo of the rail system is shown in Fig. 3. This system consisted of a 12.2-m (40-ft) long guide rail, a wheeled and motorized platform that translated along the rail, a sonar tower, and an extender. The sonar tower was attached to the platform and stood 1.76 m above the bottom. A 2.13-m (7-ft) tall extender could be inserted between the platform and sonar tower to increase its height to 3.89 m, permitting different grazing angles on the bottom.

The sonar tower held two sets of project and receive transducers as well as scanning motors for horizontal pan and vertical tilt, allowing the transducers an almost 360^o (180^o) rotational (tilt) capability. A parametric sonar and omni-directional International Transducer Corporation (ITC) 1001 transducer were used as the projector and receiver, respectively, for one set of transducers. The parametric sonar was operated in the frequency band of 1 to 20 kHz, and it produced about a 5^o conical beam (3-dB-down boundary) with side lobes more than 50-dB down from the main lobe across its operational frequency band. The ITC 1001 transducer was located next to the parametric sonar, and it was used to record the backscattered signals when the parametric sonar was operated. The second set of transducers consisted of two broad band, broad beam transducers. One of these transducers was a conical 10-cm-diameter broadband transducer that was used to project acoustic signals in the frequency range of 10 to 50 kHz. The receiver was a 10-cm high by 15-cm long broadband transducer operating in the 1 to 100 kHz band. The broadband projector, broadband receiver, and the parametric sonar were oriented such that their main response axes were perpendicular to the rail. Figure 4 shows a photo of these transducers on the sonar tower.

Fig. 3. Photo of rail system.

Fig. 4. Photo of transducers on sonar tower.

Two free-field hydrophones were deployed in the target field. One was an ITC 1001 transducer, and the other was an ITC 1089 transducer. Both transducers were attached to small stands that situated them approximately 0.6 m above the bottom and about 14 m from the rail system. The ITC 1001 transducer and ITC 1089 transducer were used to record each transmitted signal of the parametric sonar and the wide bandwidth projector, respectively, as they were translated along the rail system. Thus, they provided knowledge of the transmitted levels and of the locations of the transducers attached to the rail as they moved along the rail.

Transmitted signals were short sinusoidal pulses that were either 2 cycles long or 0.2 ms in duration. The 0.2-ms signals had a 0.02-ms taper on the leading and trailing edges to minimize ringing in the waveforms generated by the source. The received signals were amplified, filtered, and then digitized at a sample frequency of 500 kHz.

Buried target data were obtained by translating the transducers on the rail system and taking data in approximately 2.5-cm increments. Data were obtained for the various bottom configurations for 1.76- and 3.89-m transducer heights above the bottom, corresponding to grazing angles of 10^o and 20^o, respectively, which are both below the critical grazing angle.

III. RESULTS AND DISCUSSION

A. Data Reduction

MATLAB code was written to read and analyze the collected data. The data were processed and displayed in a backscattered intensity image (in dB), which is a plot of the backscatter intensity in range versus sonar location along the rail. The data acquired with the two broad band, broad beam transducers were also processed using an ω-k (wavenumber) algorithm as described by Hawkins.[7] Here the processed data, which are proportional to voltage, were mapped to the appropriate range and cross-range and used to generate a SAS image.

The data were further analyzed to determine the signal-to-noise ratio (SNR) of the buried target, in which the noise level refers to backscatter from the bottom sediment, i.e., bottom reverberation. To estimate the reverberation level, an average was taken from a patch near the target. The patch location and size was approximately the same for the two source-receive systems used. The location of this patch corresponded to an area situated approximately 0.5 m in front of the target (i.e., about 9.5 m from the rail), and the center of the patch was at the same cross-range as the geometric center of the target. For data obtained with the parametric sonar and ITC 1001 transducer, the patch was 1.6 m wide in cross-range and 1 m long in range, and for data obtained with the broadband, broad beam transducers, the patch was 2.75 m wide in cross-range and 0.75 m long in range. The different patch area ensured that the estimated reverberation levels were due to the rippled bottom and not contaminated from returns due to the buried target and from bottom areas that were not scraped. The maximum return from the target was compared with the mean estimated reverberation level to yield the SNR.

It should be noted that previous efforts have focused on determining calibrated backscatter levels from a buried sphere for data analysis and not SNR.[3] The motivation for using calibrated levels was twofold. First, the interaction of the in-sediment acoustic beam with a simple shaped target such as a sphere can be modeled using T-matrix calculations. Second, despite fairly uniform rakings with the sand scraper, the bottom's fine-scale roughness was found to exhibit significant variability. This is clearly seen in Table 1, which shows that the IMP2 measurements performed on the three similarly raked 75-cm wavelength, 2.7-cm (RMS) height ripple profiles exhibit moderate variability in the estimated fine-scale spectral parameters. This variability may lead to uncertainty in SNR predictions. However, the T-matrix formalism is not presently mature to properly model the interaction of the acoustic beam with the buried cylindrical target used in this series of measurements. As a result, SNRs are calculated.

B. Backscatter Intensity Images and Signal-to-Noise Ratio

Typical backscatter intensity images are shown in Figs. 5 and 6 corresponding to data collected with the parametric sonar and ITC 1001 transducer and the broadband, broad beam transducers. The images in both figures correspond to a 20^o grazing angle and a ripple orientation of 0^o. Fig 5a, 5b, 5c, 5d, 5e, and 5f are associated with frequencies of 1,

4, 5, 10, 15, and 20 kHz, respectively, and in each instance, the pulse length is 2 cycles long. A high amplitude return from the buried cylinder is clearly seen at a range of about 10.3 m and cross-ranges from 5 to 7 m for frequencies of 4, 5, 15, and 20 kHz. At 10 kHz, a return appears in the image at the expected location of the buried cylinder, but this return is only slightly above the surrounding bottom reverberation level. At 1 kHz, high amplitude levels appear across almost the entire displayed image (cross-range from 2 m to 7.5 m and ground range from 9 m to 13 m), and it is unclear if the buried target was detected.

The backscatter intensity images in Figs. 6a, 6b, 6c, and 6d were processed using SAS techniques and correspond to frequencies of 10, 20, 30, and 40 kHz, respectively. The buried cylinder is easily seen at 10, 20, and 30 kHz, and these images indicate a target size of about 1.5 m and an orientation of about 7^o. Both of these compare well with expected values. At 40 kHz, the buried target is observed in the image, but its level is closer to that of the background reverberation level.

Tables 2 and 3 list the measured SNRs at various frequencies for the three different ripple orientations. In both cases grazing angle was 20^o. Table 2 refers to data acquired using the parametric sonar and ITC 1001 transducer, and the transmitted pulses were 2 cycles in duration. Table 3 corresponds to data collected using the broadband, broad beam transducers in which 0.2-ms long pulses were employed, and the data were processed using SAS techniques. Trends in the tables indicate that there are two regions in which the SNR peaks across particular frequency bands. The first region corresponds to a frequency range of 1 to about 10 kHz. The second refers a region that begins near 10 kHz and ranges to about 40 to 45 kHz. In addition, the results show that for a particular frequency greater than or equal to 20 kHz, the SNR in this second region decreases with increasing ripple orientation.

The backscattered intensity plots and the listed SNR levels show that sonar performance (image quality, SNR, etc.) is dependent upon the combination of: (a) the amount of acoustic energy penetrating into the bottom, (b) the bottom reverberation levels, and (c) the sonar's resolution. Subcritical penetration is due to either evanescent transmission or ripple scattering. Previous work has indicated that evanescent transmission is important for frequencies less than 10 kHz while ripple scattering becomes the dominant mechanism for frequencies above 10 kHz.[3] This is consistent with the SNRs listed in the tables that indicate two distinct frequency regions, one region <10 kHz and the other ≥ 10kHz, in which peaks appear in the SNR. In addition, for the case where ripple scattering is the dominant mechanism, perturbation theory predicts that for a particular ripple wavelength, the cutoff frequency for subcritical penetration (where β_n=0^o in Eq. (1) and the penetrating field becomes evanescent) decreases with increasing ripple orientation, which is again consistent with measured results. For the conditions in this measurement, first-order perturbation theory predicts a cutoff frequency of approximately 39 kHz for a 20^o grazing angle and a 0^o ripple orientation. However, measurements at 40 kHz have shown SNR = 14 dB. For this case, the perturbation parameter (the product of the wavenumber and the RMS height) at 20 kHz is already 2.1, which is high enough to cause concern for low-order perturbation theory and suggests that higher-order effects need to be considered in modeling. Such results are consistent with previous measurements.[3,8]

Table 2. Measured SNRs for selected frequencies. Source is the parametric sonar.

f (kHz)	0^o SNR (dB)	17^o SNR (dB)	31^o SNR (dB)
1	<0	<0	<0
1.5	<0	<0	<0
4	8	12	13
5	9	9	---
8	10	7	---
10	7	15	---
15	15	16	---
20	21	12	---

Table 3. Measured SNRs for selected frequencies. Source is the broadband, broad beam projector.

f (kHz)	0^o SNR (dB)	17^o SNR (dB)	31^o SNR (dB)
10	13	15	17
15	21	21	21
20	27	25	19
25	25	23	16
30	26	19	14
35	21	---	---
40	14	<0	<0
45	<0	<0	<0
50	<0	<0	<0

For the case in which evanescent transmission is the dominant mechanism (i.e., less than 10 kHz), a lower frequency pulse is expected to penetrate further into sediment than one at a higher frequency. However, subcritical detection of a buried target is also impacted by bottom reverberation levels, which depend upon bottom characteristics and sonar resolution. This is shown in Table 2 and in the images in Fig. 5. Even though the sonar resolution is higher at 10 kHz than at 5 kHz, the SNR from the buried target was less at 10 kHz than at 5 kHz. This is most likely due to higher evanescent transmission at 5 kHz than at 10 kHz. On the other hand, at 1 and 1.5 kHz, it is unclear if the buried cylinder is detected. At these frequencies, the range resolution is 3 to 5 times larger than at 5 kHz, and thus, the detection is not obvious, especially when comparing to the higher frequencies where the resolution is higher. In addition, when ripples are present, scattering from the interface may be a significant source of reverberation. The frequency of the dominant scattering peak associated with rippled interface roughness readily follows from first-order perturbation theory to be

$$f = C_1 / \left(2\lambda_r \cos\theta\right), \qquad (2)$$

with C_1, λ_r, and θ as previously defined. For parameters used in this measurement, a 20° grazing angle and ripple wavelength of 75 cm, Eq. (2) predicts the scattering peak will be near 1 kHz. Bottom backscatter measurements from a rippled bottom in the 1 to 10 kHz frequency range have shown increased reverberation levels according to Eq. (2).[9] Such an increase in reverberation level may also explain why the buried target may not have been detected.

Subcritical detection performance is dependent upon sonar's resolution. This effect is observed by comparing the images of the buried cylinder appearing in Fig. 5d with that in Fig. 6a (frequency of 10 kHz) and in Fig. 5f with that in Fig. 6c (frequency of 20 kHz). For a particular frequency, the image of the buried cylinder formed from data acquired with the broadband, broad beam transducers and processed using SAS techniques produced a target image that had higher SNR and a more accurate indication of size and orientation than that generated using the parametric sonar. This is because the SAS processed data results in a significantly higher resolution, which results in less bottom reverberation levels, than the corresponding results obtained with the parametric sonar.

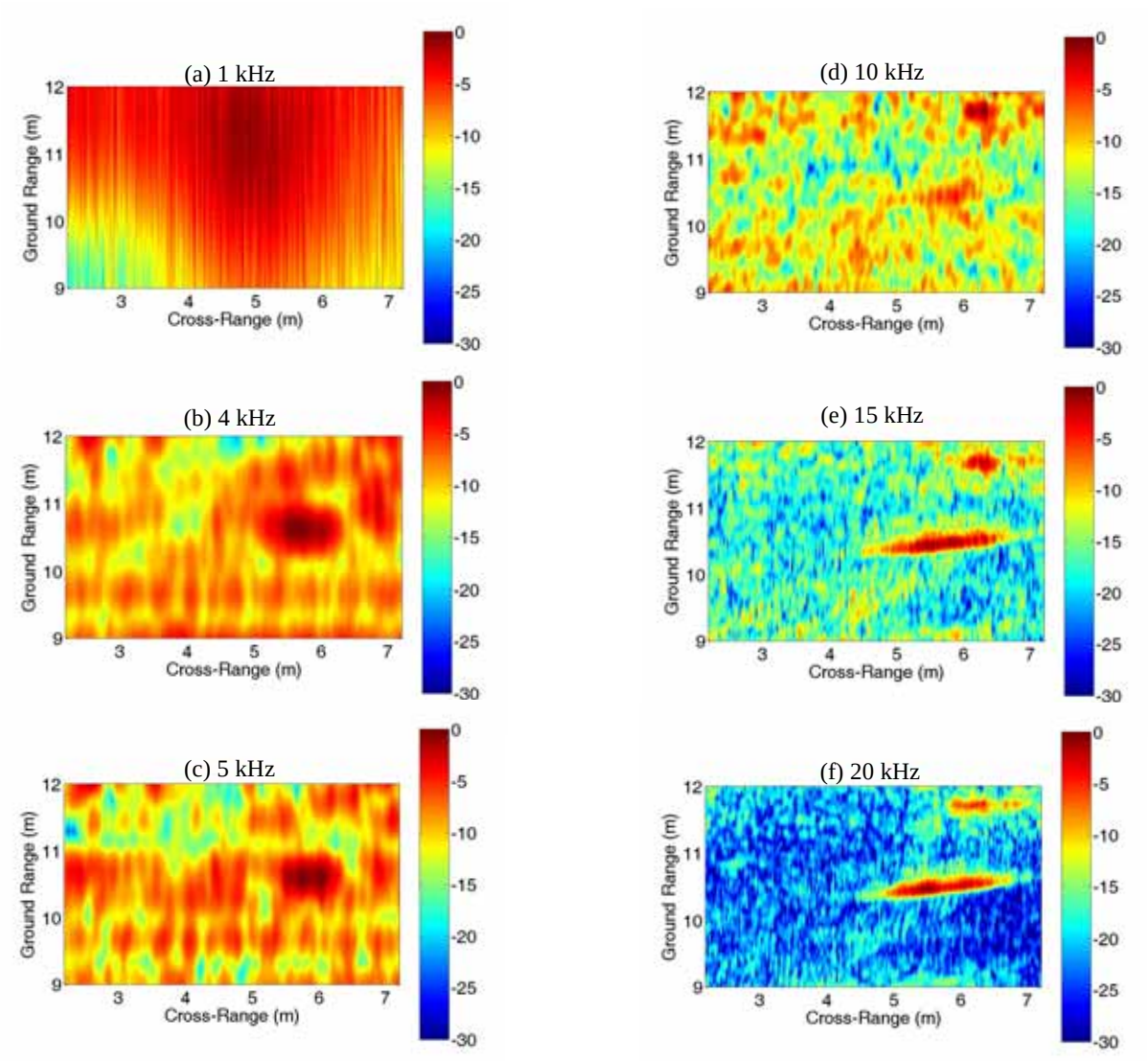

Fig. 5. Backscattered intensity images. Source is the parametric sonar.

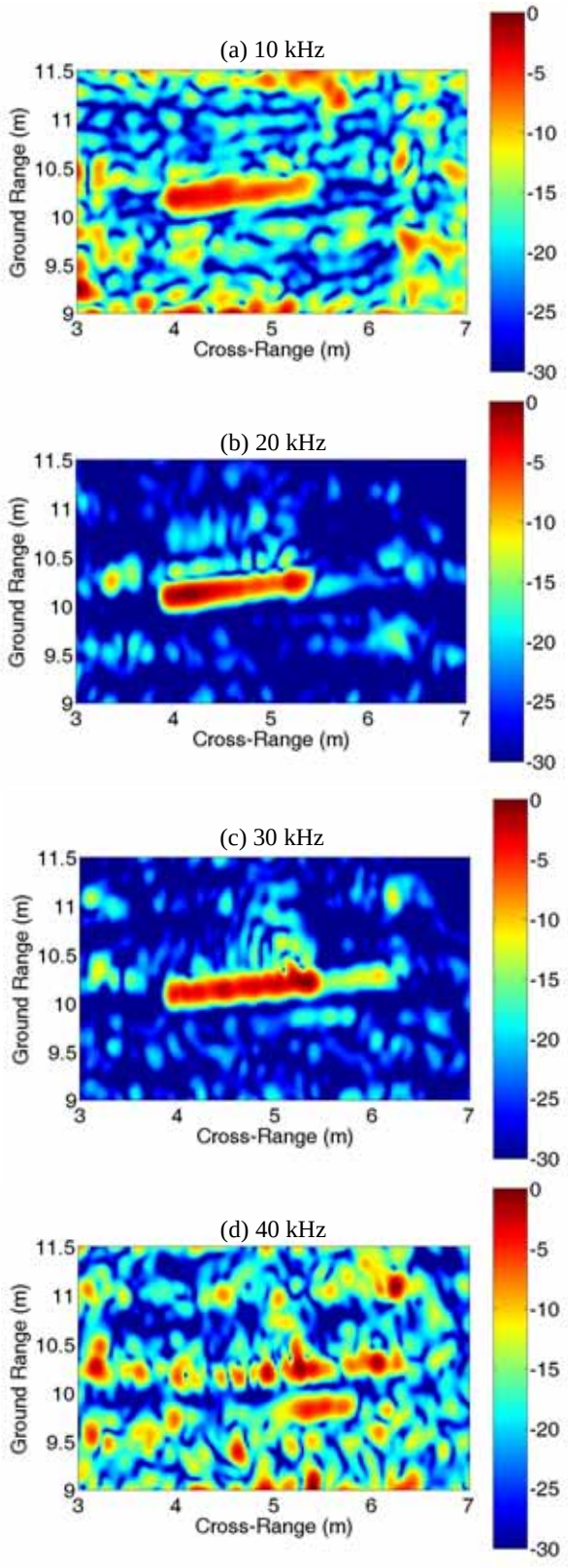

Fig. 6. Backscattered intensity images. Source is the broadband, broad beam projector.

IV. SUMMARY

A controlled set of measurements were conducted that continue previous work[2,3] studying shallow grazing angle acoustic detection of targets buried in sand having a sinusoidal, rippled sediment-water interface. In this recent effort, effects of ripple orientation on detection performance of a cylindrical target in the frequency range of 1 to 50 kHz were investigated for 10^o and 20^o incident grazing angles, which are below the critical angle. Three sinusoidal profiles corresponding to ripple orientations of 0^o, 17^o, and 31^o were formed over the buried target. Each profile was designed to have a ripple wavelength of 75 cm with an RMS height of 2.7 cm.

The results show that the buried cylinder can be detected at subcritical grazing angles via evanescent transmission for frequencies less than 10 kHz and via scattering from ripples on the sea floor for frequencies of 10 kHz and above. In addition, sonar performance (image quality, SNR, etc.) was found to be dependent upon the combination of: (a) the amount of acoustic energy penetrating into the bottom, (b) the bottom reverberation levels, and (c) the sonar's resolution. When the data were processed using SAS techniques, the generated backscatter intensity images indicated a target size and orientation comparable with the expected values. Furthermore, the results of this measurement were found to be consistent with previous published work, which suggested that when the ripple amplitude is high, higher-order effects need to be considered in modeling for the subcritical detection via ripple scattering.[3]

Future work includes: (a) completing analysis of the data, including data obtained at a 10^o grazing angle, to determine the backscattered calibrated levels from the target and the bottom sediment, (b) comparing measured SNR and backscattered intensity images to predictions of the Shallow Water Acoustic Toolset (SWAT) code,[10] and (c) conducting additional measurements to investigate detection performance under more realistic conditions, such as using ripple profiles similar to those found in coastal areas and using differently shaped/extended buried targets.

ACKNOWLEDGMENTS

The authors gratefully acknowledge support from the Office of Naval Research (ONR Codes 32OMCM, 321OE, and 321OA) and the Unexploded Ordnance Office of the Strategic Environmental Research and Development Program (SERDP) for this work. The authors also wish to thank the following for their participation and help in this effort: Ed Kloess, Dan Brown, and Dan Cook of NSWC-PC; Eric Thorsos, Kevin Williams, Dajun Tang, Vern Miller, Paul Aguilar, and Eric Boget of the Applied Physics Laboratory, University of Washington.

REFERENCES

[1] D. R. Jackson, K. L. Williams, E. I. Thorsos, and S. G. Kargl, “High-frequency subcritical acoustic penetration into a sandy sediment,” *IEEE J. Ocean. Eng.*, **27**, 346-361 (2002).

[2] J. L. Lopes, C. L. Nesbitt, R. Lim, D. Tang, K. L. Williams, and E. I. Thorsos, “Shallow Grazing Angle Sonar Detection of Targets Buried Under a Rippled Sand Interface,” Proceedings of Oceans 2002 MTS/IEEE, pp. 461-467.

[3] J. L. Lopes, C. L. Nesbitt, R. Lim, K. L. Williams, E. I. Thorsos, and D. Tang, "Subcritical Detection of Targets Buried Under a Rippled Interface: Calibrated Levels and Effects of Large Roughness," Proceedings of Oceans 2003 MTS/IEEE, pp. 485-493.

[4] K. L. Williams, D. R. Jackson, E. I. Thorsos, and D. Tang, “Comparison of sound speed and attenuation measured in a sandy sediment to predictions based on the Biot theory of porous media,” *IEEE J. Ocean. Eng.*, **27**, 413-428 (2002).

[5] D. Tang, K. B. Briggs, K. L. Williams, D. R. Jackson, and E. I. Thorsos, “Fine-scale volume heterogeneity measurements in sand,” *IEEE J. Ocean. Eng.*, **27**, 546-560 (2002).

[6] K. B. Briggs, D. Tang, and K. L. Williams, “Characterization of interface roughness of rippled sand off Fort Walton Beach, Florida,” *IEEE J. Ocean. Eng.*, **27**, 505-514 (2002).

[7] D. E. Hawkins, *Synthetic Aperture Imaging Algorithms: with Application to Wide Bandwidth Sonar*, Ph.D. Dissertation, University of Canterbury, Christchurch, New Zealand, October 1996.

[7] J. E. Moe and D. R. Jackson, “Near-field scattering through and from a 2-D fluid-fluid rough interface,” *J. Acoust. Soc. Am.* **103**, 275-287 (1998).

[8] J. E. Piper, K. W. Commander, E. I. Thorsos, and K. L. Williams, "Detection of buried targets using a synthetic aperture sonar," IEEE J. Ocean. Eng., 27, 495-504 (2002).

[9] J. L. Lopes, R. Lim, and K. Commander, “Mid Frequency Sonar Backscatter Measurements from a Rippled Bottom,” High Frequency Ocean Acoustics Conference, La Jolla, CA, March 2004.

[10] G. S. Sammelmann, "High Frequency Images of Proud and Buried 3-D Targets,” Proceedings of Oceans 2003 MTS/IEEE, pp. 266-272.